Switches to slow rhythmic neuronal activity lead to a plasticity-induced reset in synaptic weights

Abbreviated title
Brain state-dependent reset in synaptic connections

Authors
Kathleen Jacquerie, Caroline Minne, Juliette Ponnet, Nora Benghalem, Pierre Sacré, and Guillaume Drion

Author affiliations
Department of Electrical Engineering and Computer Science, University of Liège, Allée de la découverte, 10, 4000, Liège, Belgium

Author contributions
K.J. and G.D. conceived the project. K.J. and C.M. performed the computational experiments. K.J. and J.P. performed the analytical demonstrations for biophysical models and the associated simulations. P.S. and N.B. performed the analytical demonstrations for the phenomenological models and the associated simulations. K.J., C.M., P.S. and G.D. wrote the paper.

Corresponding authors
Kathleen Jacquerie: kathleen.jacquerie@uliege.be

Conflict of interest
The authors declare no conflict of interest.

Acknowledgments
Kathleen Jacquerie is a Research Fellow of the Fonds de la Recherche Scientifique - FNRS. We thank Danil Tyulmankov from Columbia University for helpful discussions and comments.

Keywords
synaptic plasticity, *STDP*, *calcium-dependent plasticity*, *brain states*, *neuromodulation*, *homeostasis*, *excitability*, *memory consolidation*

Abstract

Memory formation relies on changes in synaptic connections via synaptic plasticity, which is driven by neuronal activity. Simultaneously, behavior is controlled by switches in brain states: quiet waking is characterized by large low-frequency fluctuations in cortical activity that are strongly suppressed during active waking. We use computational modeling to study how switches in brain states interact with memory formation. We show that the low-frequency rhythmic bursting activity reminiscent of quiet waking induces a reset in synaptic weights. This reset occurs regardless of the implemented synaptic plasticity rule, whether phenomenological or biophysical, and is robust to biological variability and network heterogeneity. Mathematical analysis shows that the reset is rooted in the endogenous nature of the low-frequency quiet waking rhythmic activity. This brain state-dependent reset in synaptic weights restores the ability to learn through synaptic plasticity rules between periods of active waking, which could be a key component of memory homeostasis.

Introduction

Our brain has the ability to quickly adapt our behavior to incoming events from the environment, as well as to learn from experience to shape our memory. This behavioral control is built on fluctuations in neuronal patterns at the cellular and population levels, defining different *brain states* (Buzsáki, 1998; Cannon et al., 2014; Jacquerie and Drion, 2021). These patterns are spatiotemporal signatures of large neuronal populations and synaptic activity. While global and long-lasting switches between different brain states have been observed during wake-sleep transitions for some time (McCormick and Salkoff, 2015; Sherman, 2001), it is becoming more and more clear that fast and localized switches in brain states actively control behavior during wakefulness. Specifically, a large, low-frequency rhythmic activity in the local field potential (LFP) or in the electroencephalogram (EEG) is observed during quiet waking, but suppressed during active waking (Kühn et al., 2004; McGinley et al., 2015; Dastgheib et al., 2022; Vyazovskiy et al., 2011). At the neuronal level, this low-frequency rhythmic activity observed during quiet waking emerges from rhythmic *bursting*, whereas active waking is characterized by asynchronous *tonic spiking* (Zagha and McCormick, 2014).

In parallel, memory relies on *synaptic plasticity*, which is the ability of neurons to modify their connections with other cells (Citri and Malenka, 2008; Heidelberger et al., 2014). Two categories of synaptic plasticity rules are often encountered in the literature: those that consider spike time series as input, (Pfister and Gerstner, 2006; Song et al., 2000) and those that use calcium as a key driver (Shouval et al., 2002; Graupner and Brunel, 2012). Although the validity and role of these rules in shaping how a neuronal network learns specific tasks have been extensively studied, our understanding of how such rules interact with the fluctuations in brain states is still scarce (Olcese et al., 2010; González-Rueda et al., 2018; Fauth and Van Rossum, 2019).

In this paper, we investigate how network switches from asynchronous tonic spiking to rhythmic bursting, as those observed when transitioning from active to quiet waking, affect the outcome of several synaptic plasticity rules. To this end, we construct a neuronal circuit capable of rapidly switching between these two firing patterns under the action of neuromodulators. This circuit is made of conductance-based model neurons and comprises an inhibitory neuron that projects onto excitatory neurons. The synaptic connections between the excitatory neurons are governed by a synaptic plasticity rule. We compare 20 different rule variations, ranging from spike-time dependent plasticity rules (such as pair-based and triplet (Song et al., 2000; Van Rossum et al., 2000; Pfister and Gerstner, 2006)) to calcium-dependent rules (Shouval et al., 2002; Graupner et al., 2016; Deperrois and Graupner, 2020). All rules are parameterized to fit experimental data obtained either on a spike-timing protocol (Bi and Poo, 1998) or on a frequency-pairing protocol (Sjöström et al., 2001). We then compare how strong and weak synaptic weights acquired during tonic spiking, associated with active waking, evolve as the network switches into rhythmic bursting mode, associated with quiet waking.

A switch to rhythmic bursting mode results in a reset of synaptic weights: whatever the strength established during active waking, the network resets its connectivity to a single steady-state value

during quiet waking, regardless of the implemented plasticity rule. We refer to this process as a *homeostatic reset* of synaptic weights, as it fully relies on endogenous network properties and promotes the synaptic weight restoration during quiet wakefulness. The homeostatic reset is shown to be robust to the level of neuromodulation, and to both variability and heterogeneity in circuit parameters. Further analytical investigations show that the mechanisms underlying the reset are rooted in the interactions between the endogenous dynamics of network rhythmic bursting activity and the plasticity rules themselves, both being largely independent of initial synaptic weights.

Materials and Methods

Conductance-based modeling

All neurons are modeled using a single-compartment Hodgkin and Huxley formalism. The membrane voltage V_m evolves as follows (Drion et al., 2018; Jacquerie and Drion, 2021):

$$C_\mathrm{m}\dot{V}_\mathrm{m} = -\sum_i I_{\mathrm{ion},i} + I_\mathrm{app}$$

where C_m is the membrane capacitance, $I_{\mathrm{ion},i}$ is the ith current carried by ionic channels ion, and I_app is an external applied current. The description of the ionic currents and the associated parameters are described in *SI Appendix*.

The neuron circuit is composed of three neurons (see Figure 1). The two excitatory neurons are connected through a feedforward AMPA synapse where the afferent neuron is referred to as the presynaptic (pre) neuron, and the efferent neuron as the postsynaptic (post) neuron. An inhibitory neuron (I) is connected to two excitatory neurons through $\mathrm{GABA_A}$ and $\mathrm{GABA_B}$ connections. The synaptic currents are described in *SI Appendix*.

The inhibitory cell controls the state of the circuit. A tonic firing in the inhibitory neuron puts the two excitatory cells in a resting state. If the pre- or postsynaptic cell receives a external depolarizing pulse, it generates an action potential. A hyperpolarizing current applied to the inhibitory neuron switches the whole circuit into rhythmic bursting mode. This hyperpolarizing current models the effect of a neuromodulator signal (NMOD) (Zagha and McCormick, 2014).

Synaptic plasticity

The synaptic AMPA connection between the presynaptic neuron and the postsynaptic neuron is subjected to plasticity. The time evolution of this connection is studied during both tonic and bursting modes. This AMPA synapse is modeled by $g_\mathrm{AMPA}(t) = w(t)\ \bar{g}_\mathrm{AMPA}$ where $w(t)$ the synaptic weight, and $\bar{g}_\mathrm{AMPA}$ is the constant maximal conductance. A very small initial connectivity $\bar{g}_\mathrm{AMPA}$ equal to $0.01\,\mathrm{mS/cm^2}$ is taken such as the induced Excitatory Post-Synaptic Potential (EPSP) at the postsynaptic site does not initiate a spike. The variable $w(t)$ is weighing the synaptic current and is driven by a synaptic plasticity rule.

Two main categories of synaptic plasticity rules are explored in this paper: phenomenological rules and calcium-based rules (Gerstner, 2011; Gerstner and Kistler, 2002). The first category uses the pre- and postsynaptic spike times to drive the synaptic change while the second category uses the calcium signal.

Phenomenological models

The pair-based model considers the pre- and postsynaptic spike time (resp. t_pre and t_post) with a time difference $\Delta t = t_\mathrm{post} - t_\mathrm{pre}$ to induce the change in synaptic weight. To reproduce the classical STDP window, a pair-based model was implemented (Abbott and Nelson, 2000; Song et al., 2000; Morrison et al., 2008; Rubin et al., 2001; Van Rossum et al., 2000):

$$w \to \begin{cases} w + A^+(1-w)^\mu e^{-\Delta t/\tau^+}, & \text{at } t_\mathrm{post} \text{ if } t_\mathrm{pre} < t_\mathrm{post}, \\ w - A^- w^\mu e^{\Delta t/\tau^-}, & \text{at } t_\mathrm{pre} \text{ if } t_\mathrm{pre} > t_\mathrm{post}, \end{cases}$$

where $A^+ > 0$, $A^- > 0$ (Morrison et al., 2008; Song et al., 2000). The weight dynamics can be constrained in two manners; either by using *hard bounds* or *soft bounds*. Hard bounds permits to stop the weight increase or decrease by adding upper or lower limits. Soft bounds decelerates the evolution if the weight reaches a bound. It is modeled by the weight-dependency parameter μ: μ is equal to 0 for hard-bounds and to 1 for soft-bounds) (Gerstner and Kistler, 2002).

The functions $e^{-|\Delta t|/\tau^{\pm}}$ are the temporal kernel of potentiation and depression. If we introduce $S_{\text{pre}}(t) = \sum_k \delta(t - t_{\text{pre},k})$ and $S_{\text{post}}(t) = \sum_k \delta(t - t_{\text{post},k})$ for the spike trains of pre- and postsynaptic neurons, the evolution of the synaptic weight can be written as follows:

$$\dot{w} = -A^- w^\mu \left[\int_{-\infty}^{0} e^{s/\tau^-} S_{\text{post}}(t-s)ds\right] S_{\text{pre}}(t) + A^+(1-w)^\mu \left[\int_{0}^{\infty} e^{-s/\tau^+} S_{\text{pre}}(t-s)ds\right] S_{\text{post}}(t). \quad (1)$$

The triplet-based model extends the pair-based model to account for three spikes patterns, such as pre-post-pre and post-pre-post (Pfister and Gerstner, 2006). We implemented both pair and triplet using trace variables following (Pfister and Gerstner, 2006). More details are provided in *SI Appendix*.

Biophysical models

We modeled calcium dynamics by following (Graupner and Brunel, 2012; Graupner et al., 2016). The global equation for the calcium-dependent plasticity rule is written as

$$\tau_w([\text{Ca}])\dot{w} = \Omega([\text{Ca}]) - \mu\, w, \quad (2)$$

where μ modulates the weight-dependency: $\mu = 0$ (resp. $\mu = 1$) refers to hard (resp. soft) bounds. In total, we have investigated five major calcium-based dependent models in this paper. Some rules were adapted to fit either *frequency-dependent protocol* (cortical experimental data (Sjöström et al., 2001)) or a *STDP* protocol (hippocampus experimental data (Bi and Poo, 1998)). Different *weight-dependencies* (soft bounds or hard bounds) are compared. The impact of the *coupling* between the presynaptic calcium influx and the synaptic weight or the presence of *short-term depression* are also tested (Deperrois and Graupner, 2020). Calcium-based rules are either implemented using two-triggered calcium thresholds for potentiation and depression, or using a continuous function for calcium dependency. More details are provided in *SI Appendix*.

Computational experiments

Figure 1A shows the local field potential (LFP) in a circuit composed 6 excitatory neurons connected to 6 other excitatory neurons. They all receive an inhibitory current from the inhibitory cell. The local field potential measures the average behavior of interacting neurons (Jacquerie and Drion, 2021; Mazzoni et al., 2015; Telenczuk et al., 2020). It reflects the collective excitatory synaptic activity received by the postsynaptic neuron population. The postsynaptic current from neuron i to neuron j is $I_{\text{syn,j}}(t) = -\bar{g}_{\text{AMPA}} w_{ij}(t) s_{\text{AMPA}}(V_m - 0)$. The overall synaptic activity is measured by the mean of the individual synaptic current $\text{LFP}(t) = 1/6 \sum_{j=1}^{6} I_{\text{syn,j}}(t)$.

Figure 1B simulates two switches from tonic activity followed by bursting activity of 40 s each for 6 neuronal circuits. Among these 6 circuits, three of them have a correlated tonic firing while the three other circuits have uncorrelated tonic firing. For correlated circuits, the two excitatory neurons are tonically spiking at high frequencies with close pre-post pairs of spike. This activity correlation induces an increase in synaptic weight. For uncorrelated circuits, pre and post cells fire independently at the same nominal frequency f_0. Spike timings are generated with interspike intervals following independent Normal distributions $\mathcal{N}(\frac{1}{f_0}, (\frac{0.3}{f_0})^2)$. During burst firing, the level of neuromodulators is modeled by a hyperpolarizing current applied to the inhibitory neuron (more details in *SI Appendix*). The synaptic plasticity rule is the triplet rule (Pfister and Gerstner, 2006).

In Figure 3A, the variability in neuromodulator concentrations (shades of gray) is obtained by varying the hyperpolarizing current value applied to the inhibitory cell, ranging from -1 to $-1.7\,\text{nA/cm}^2$ resulting in different bursting patterns (see all traces in *SI Appendix, Fig.S5*). Figure 3B depicts the mean of the synaptic weight time evolution for 10 circuits in which variability in the ionic conductances

is added. Each circuit is initialized with maximal conductances that are randomly picked from a Uniform distribution on an interval of 10 % around its nominal value $\bar{g}_0$, such as $[\bar{g}_0 - 0.1\bar{g}_0, \bar{g}_0 + 0.1\bar{g}_0]$. The plasticity rule used is the calcium model from (Graupner et al., 2016). Figure 3C considers a network of 2 layers with 100 presynaptic neurons fully connected to 100 postsynaptic neurons in a feedforward configuration. The connections (colors) are initialized randomly between 0 and 1. Intrinsic parameters of all cells are randomized by adding variability in the ionic conductances $g_{\mathrm{K,Ca}}$ and $g_{\mathrm{Ca,T}}$ in the same way as in the Figure 3B, with 20 % variability. The plasticity rule used is the calcium model from (Graupner et al., 2016).

Synaptic weight equilibrium value can be found by analytical demonstration (see in *SI Appendix* for details).

Figure 4A shows the kernel of pair-based plasticity rule considering the synaptic weight-dependency. It unravels the effective value of the potentiation and depression increment respectively labeled $A^+(1-w)$ and A^-w. Figure 4C (left) gives the ratio between the positive and negative correlation. The positive correlation describes the correlation for a presynaptic spike followed by a postsynaptic spike. The negative correlation describes the inverse relation for a postsynaptic spike followed by a presynaptic spike. Figure 4C (right), the simulated value is equal to the converging value in the time evolution of the synaptic weight. The predicted value is computed from the analytical formula provided w_{HR}.

Figure 5A shows the kernel of the pair-based plasticity rule (top, left) and calcium-based rule (bottom, left) with potentiation and depression parameters that are affected by neuromodulators. The evolution of the synaptic weights during bursting activity is shown in Figure 5A when the initial weight is tested between 0 and 1 (right). Blue curves are obtained using the traditional synaptic rule and yellow curves are obtained using the neuromodulated synaptic plasticity rule. Figure 5B shows the same experiment but the parameters are dependent on the initial synaptic weights to mimic tag-dependency. We consider a strong weight when at the end of the learning phase the weight is greater than 0.75 setting the threshold tag value. Figure 5C reproduces the computational experiment presented in Figure 1. Six neuronal circuits are tested during 2 cycles of tonic-burst activity (each state lasts 30 s). For correlated circuits (dark blue), each neuron fires independently at a frequency higher than 30Hz. For uncorrelated circuits (light blue), each neuron fires at a low value. During burst, the inhibitory neuron is hyperpolarized. At the second burst phase, the plasticity rule is neuromodulated (Figure 5C) or neuromodulated and tag-dependent (Figure 5D).

More details on all computational experiments can be found in *SI Appendix*. Simulations were performed using the Julia programming language (Bezanson et al., 2017). Analyses were performed either in Matlab. Code files are freely available at `https://github.com/KJacquerie/HomeostaticReset`.

Results

Switches to a rhythmic bursting reminiscent of quiet waking lead to a homeostatic reset of synaptic weights

We first investigated how switches in brain states, neuromodulation of activity, and synaptic plasticity interact by implementing a pair-based rule from (Pfister and Gerstner, 2006) in a neuron circuit capable of switching between asynchronous tonic spiking and rhythmic bursting states (Drion et al., 2018; Jacquerie and Drion, 2021). The neuron circuit follows a conductance-based modeling paradigm and reproduces the activities observed in cortical networks during switches in brain states (McCormick and Bal, 1997; Zagha and McCormick, 2014; Chrol-Cannon and Jin, 2014), among others. The circuit comprises an inhibitory neuron that projects GABAergic currents onto two excitatory neurons, which are connected by an AMPAergic current (Figure 1A, left). This 3-cell circuit provides an appropriate support to study the transition between several firing patterns and its functional consequence on the evolution of synaptic weight. Indeed, this topology is often encountered in different brain regions; such as the thalamus between reticular and relay cells (Steriade et al., 2001; Sherman and Guillery, 1996), the cortex between pyramidal and inhibitory cells (Bazhenov et al., 2002; Hill and Tononi, 2005), or even between different organs like striatum and basal ganglia (Humphries, 2012; Kühn et al., 2004). Applying a hyperpolarizing current to the inhibitory cell, which models the effect of neuromodulators (NMOD, Figure 1A), switches the whole circuit from tonic firing to synchronous bursting (Figure 1A, right).

The LFP is computed in a network of 6 excitatory neurons connected to 6 postsynaptic neurons. It measures the average synaptic activity in the network. The transition from tonic to burst at the cellular level is translated by the marked transition from the low amplitude, high frequency activity to a large, low-frequency rhythmic activity. It mimics e.g. the type of switches observed during transitions from active to quiet waking (Reimer et al., 2014; McGinley et al., 2015; Zagha, 2014; Dastgheib et al., 2022).

We then implemented a synaptic plasticity rule between the two excitatory neurons in the circuit. The connection strength between the neurons, or synaptic weight, is characterized by a variable w (Figure 1A). Synaptic plasticity is modeled by a synaptic rule describing the evolution of the synaptic weight throughout time (Figure 1A, right). We used a classical triplet model as the synaptic plasticity rule in this neuronal model due to its prevalence in the literature (Pfister and Gerstner, 2006). The rule parameters was fitted on the well-established experimental data obtained through a frequency pairing protocol (Sjöström et al., 2001) (more details on the parameter model fitting see *SI Appendix*).

To investigate how fast switches in firing patterns affect synaptic connections in the presence of the triplet model, we subjected six circuit models to two transitions from active to quiet waking and back (ie. from tonic spiking to bursting), while letting the plasticity rule run its course (Figure 1B). Among these six circuits, three were designed to exhibit a correlated activity between the excitatory neurons with the presynaptic neuron firing slightly before the postsynaptic neuron, mimicking the activity of neurons receiving functionally related inputs (dark blue curves in Figure 1B). The three others were designed to exhibit an uncorrelated, random activity, mimicking the activity of neurons receiving unrelated inputs (light blue curves in Figure 1B). We then compared the evolution of the synaptic weight in these six circuits along the two transitions from tonic firing to burst firing (see middle panel of Figure 1B).

During active waking, neurons are in tonic firing mode and the synaptic weights evolve according to the level of correlation between the presynaptic and postsynaptic neurons, consistent with the triplet rule. The connection strengths between neurons exhibiting correlated activities increase(Figure 1B, top left), whereas the connection strengths between neurons exhibiting uncorrelated activities decrease (Figure 1B, bottom left).

As the circuit switches to quiet waking, the neurons switch to a rhythmic, low-frequency bursting mode. This change in activity radically affects the time evolution of the synaptic weights under the triplet rule: connections that were potentiated during the previous active tonic firing phase start to depress (Figure 1B, top right), whereas connections that were depressed start to potentiate (Fig-

ure 1B, bottom right), and all connection strengths eventually converge to a single, stable point. This convergence point is fully independent of what happened during learning. We call this phenomenon a *homeostatic reset* of synaptic weights, as it relies on a switch to an endogenous, rhythmic bursting activity of the network and his independent from external inputs and learning history.

The potential functional consequences of the homeostatic reset are twofold. On the one hand, it promotes the restoration of synaptic weights during periods of quiet waking, which in turn restores the ability to learn new information. On the other hand, it disrupts any learning that may have occurred during the previous active waking, if one solely relies on the evolution of w under the triplet rule.

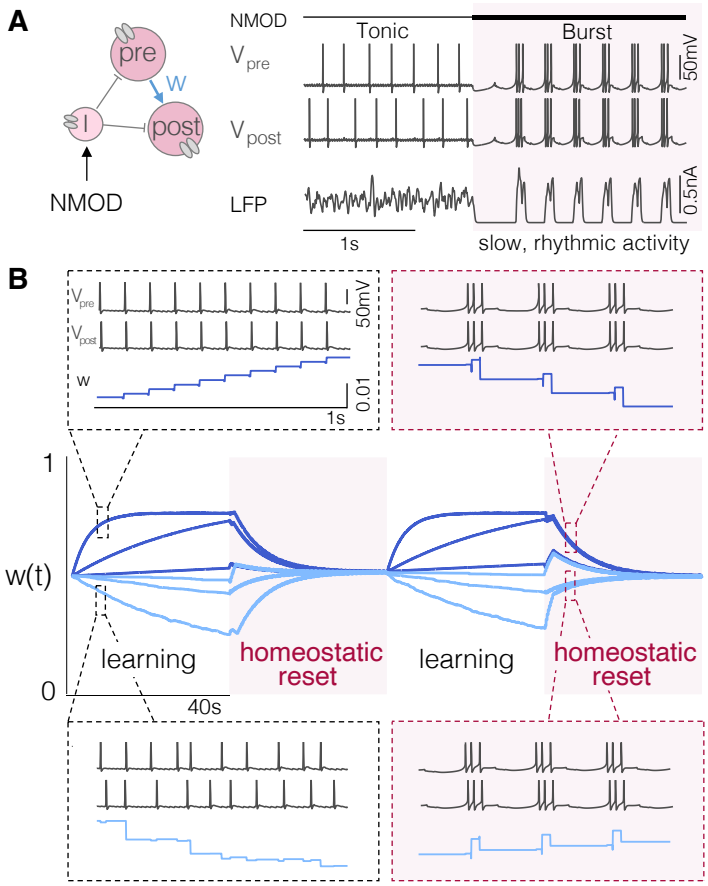

Figure 1: A homeostatic reset of synaptic weights is observed during rhythmic bursting mode whatever the neuronal activity correlation in tonic spiking

A. (Left) scheme of the three-cell circuit. The circuit is composed of an inhibitory cell (I) that projects GABA current onto excitatory pre- and postsynaptic neurons (resp. pre and post), which are connected by AMPA currents. The synaptic strength between pre-post w s is governed by a triplet rule. (Right,top) Applying neuromodulators (NMOD) onto the I-cell induces the transition from tonic to burst in the circuit. (middle) Membrane potential of the pre- and postsynaptic neurons. on tonic mode (white background), and rhythmic bursting mode (pink background). (bottom) Local Field Potential (LFP) recordings in a network of 6 postsynaptic neurons. Transition to neuronal bursting activity appears as high amplitude and low frequency rhythmic LFP.

B. Evolution of the synaptic weight in 6 circuits during two brain state transitions. During tonic firing (white background), 3 circuits have a strong, resp. weak, correlated activity between pre- and post-synaptic neurons resulting in a synaptic weight increase, resp. decrease, shown in dark, resp. light, blue. During burst firing (pink background), all the synaptic weights are reset to the same value — a phenomenon that we called the *homeostatic reset*. Top and bottom panels provide zooms on the voltage traces and the associated synaptic weight evolution during spiking mode (learning) and bursting mode (homeostatic reset).

The homeostatic reset occurs in both phenomenological and biophysical models of synaptic plasticity

So far, we have seen that a classical triplet rule leads to a homeostatic reset in synaptic weights during a switch in network state from active waking to quiet waking referring to a cellular switch from tonic to burst. We further investigated the generality of the homeostatic reset by testing 20 variations of 7 published synaptic plasticity models. These synaptic plasticity models can be split into two categories (Figure 2A). The first category comprises phenomenological models, which use spike timing of presynaptic and postsynaptic neurons as the main input that drives changes in synaptic weights. Prominent examples of such models are the pair-based rule using the pre- and post-spiking times (Song et al., 2000; Van Rossum et al., 2000) and the triplet rule using pre-post-pre- or post-pre-post-spiking activity to change the synaptic weight (Pfister and Gerstner, 2006; Graupner et al., 2016) (Figure 2A, left blue box). The second category comprises biophysical models, which use intracellular calcium concentration as the key signal that drives synaptic change (Graupner et al., 2016; Graupner and Brunel, 2012; Shouval et al., 2002; Deperrois and Graupner, 2020) (Figure 2A, right blue box). The two representations into the blue boxes are simplified to provide a comprehensive overview of the rules. Their computational implementations are described in *SI Appendix*. Then, we compare two different *weight-dependency plasticity* for each category of model by implementing either hard bounds or soft bounds (van Rossum et al., 2012; Gütig et al., 2003).

Altogether, 2 classes of phenomenological rules (see Table 1) and 5 classes of calcium-dependent plasticity rules (see Table 2) are studied in this paper. For each class, the parameter set is related to a region, a pairing protocol, a type of bound listed in Tables 1 and 2. This raised the issue that fitting plasticity rule is a complex problem. The paper aiming at comparing the general behavior of plasticity rules during switches from tonic to burst firing, we first fitted all 20 model variations based on two well-established experimental plasticity induction protocols (Figure 2B). In the first induction protocol, the time lag between pre- and postsynaptic spikes is tested for a given frequency after several pairs. This protocol reproduces the experiment done in (Bi and Poo, 1998). Figure 2C shows the average (black curve) and standard deviation (gray shadow) of the behavior of the different models after parameterization, together with the experimental data of (Bi and Poo, 1998) (circles). In the second induction protocol, a fixed time lag is maintained while the impact of the stimulation frequency is varied. Similarly, Figure 2D shows the average (black curve) and standard deviation (gray shadow) of the behavior of the different models after parameterization for the second protocol, together with the experimental data (Sjöström et al., 2001) (circles). For each model, a specific datasheet provides the parameter values as well as the validation on experimental data and the evolution of the synaptic weight during burst mode (see *SI Appendix*).

Name	Region	Bounds	Reference	ID
Pair-based	H	Soft	(Van Rossum et al., 2000)	1
	H	Hard	(Song et al., 2000)	2
Triplet	H	Soft	adapted from (Pfister and Gerstner, 2006)	3
	H	Hard	(Pfister and Gerstner, 2006)	4
	C	Soft	(Graupner et al., 2016)	5
	C	Hard	(Pfister and Gerstner, 2006)	6

Table 1: Phenomenological models covered in this paper. Region is linked to the parameter choice depending on the brain area where the rule is fitted: (C) cortex, (H) hippocampus. The weight-dependency is either modeled by (Soft) soft bounds or (Hard) hard bounds.

We generalized the computational experiment performed in Figure 1B to all 20 synaptic model variations (see *SI Appendix* for a simulation trace of each individual simulation). In all model configurations, implementing a soft bound, a network switch from tonic spiking to bursting generated a homeostatic reset of synaptic weights, very reminiscent of what is shown in 1B. In all model configurations implementing a hard bound, a network switch from tonic spiking to bursting generated a convergence of the synaptic weights towards the extreme value with a constant velocity whatever its initial weight. Such saturation phenomenon of all synaptic weights was previously shown in other

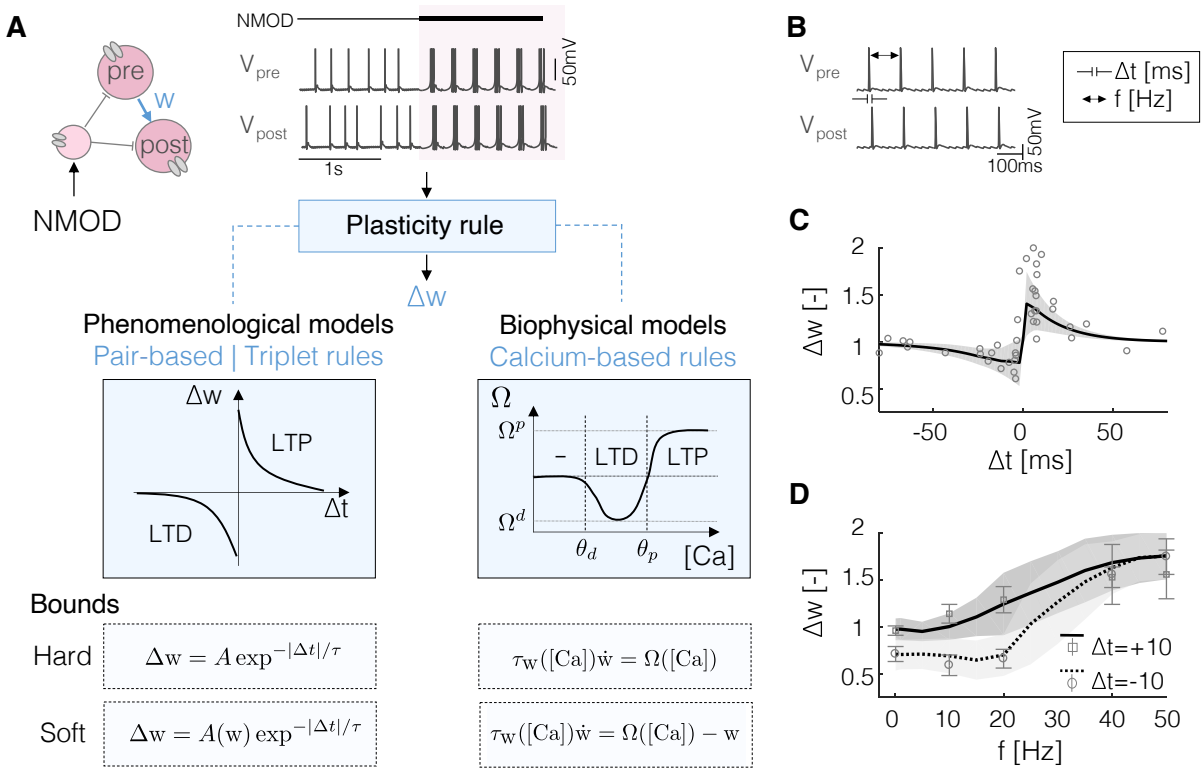

Figure 2: Two categories of synaptic plasticity rules reproduce experimental data from plasticity-induced protocol.
A. The three-cell circuit able to switch from tonic to burst. The synaptic weight w between pre- and postsynaptic neurons is affected by plasticity. Two categories of plasticity rules are tested. (Left) *Phenomenological models* focusing on the spike timing such as the pair-based and triplet models (Abbott and Nelson, 2000; Pfister and Gerstner, 2006; Graupner et al., 2016) such as $w \to w + \Delta w$ and $\Delta t = t_{\text{post}} - t_{\text{pre}}$ provoking Long-Term Depression (LTD) or Long-Term Potentiation (TOP). The weight-dependency is affecting the potentiation/depression parameter A. (Right) *Biophysical models* use the intracellular calcium to drive synaptic change such as $\tau_w([\text{Ca}])\dot{w} = F(w, [\text{Ca}])$. Intermediate (resp. high) calcium level leads to slow (resp. fast) depression (resp. potentiation). Either the plasticity rule is a continuous function of calcium (as in (Shouval et al., 2002)) or use depression and potentiation levels (Ω^{d} and Ω^{p}) associated to two calcium thresholds (depression or potentiation θ_{d} or θ_{p}), as in (Graupner et al., 2016)). The weight-dependency modifies the synaptic plasticity equation.
B. Plasticity induced protocols focus on maintaining either the simulation frequency and varying the pre- and post-spike time $\Delta t = t_{\text{post}} - t_{\text{pre}}$ (Bi and Poo, 1998) or maintaining a constant time lag and varying the spike frequency f (Sjöström et al., 2001).
C. The change of synaptic strength (Δw) is shown as a function of the pre-post pairings (Δt) for a frequency of 1 Hz, reproducing (Bi and Poo, 1998) experimental data (circles). The fit obtained in all models for hippocampus data is averaged. The mean (black line) and the standard deviation (gray shadow) are shown.
D. The change of the synaptic strength is shown as a function of frequency pairings for regular pre-post pairs ($\Delta t = 10$ ms (full line) and $\Delta t = -10$ ms (dotted line) reproducing (Sjöström et al., 2001) experimental data obtained in cortex (circles, squares, mean + std). The fit obtained in all models is averaged. The mean and standard deviation are shown by the black line and the gray shadow, respectively.

applications (Chen et al., 2013). Although the convergence dynamics are different between the two cases, the outcome is the same: a switch to bursting restores synaptic weights, potentially disrupting any learning that might have occurred during the active waking period (characterized by tonic spiking). This shows that such homeostatic reset of synaptic weights observed during switches in brain states is a robust phenomenon that does not depend on the specifics of any synaptic plasticity model.

Model	Formalism	Region	Bounds	Ca^{2+}-coupling	STD	Reference	ID
Graupner 2016	Th*	C	Soft	No	No	(Graupner et al., 2016)	1
	Th	C	Soft	No	No	adapted from (Graupner et al., 2016)	2
	Th	H	Soft	No	No	adapted from (Graupner et al., 2016)	3
	Th	C	Hard	No	No	adapted from (Graupner et al., 2016)	9
Graupner 2012	Th	C	Soft	No	No	(Graupner and Brunel, 2012)	4
	Th	H	Soft	No	No	(Graupner and Brunel, 2012)	5
Shouval 2002	Cont	C	Soft	No	No	adapted from (Shouval et al., 2002)	6
	Cont	C	Hard	No	No	adapted from (Shouval et al., 2002)	10
Deperrois 2020	Th	C	Soft	Yes	No	(Deperrois and Graupner, 2020)	7
	Th	C	Hard	Yes	No	adapted from (Deperrois and Graupner, 2020)	11
	Cont	C	Hard	Yes	No	adapted from (Deperrois and Graupner, 2020)	12
Deperrois 2020	Th	C	Soft	Yes	Yes	(Deperrois and Graupner, 2020)	8
	Th	C	Hard	Yes	Yes	adapted from (Deperrois and Graupner, 2020)	13
	Cont	C	Hard	Yes	Yes	adapted from (Deperrois and Graupner, 2020)	14

Table 2: Biophysical models investigated in this paper. (Th*) stands for calcium thresholds such as two opposing calcium-triggered pathways leading increases or decreases of synaptic strength (Graupner et al., 2016; Graupner and Brunel, 2012; Deperrois and Graupner, 2020). (Th) uses calcium-dependent steady state value and time-constant. (Cont) stands for the continuous function of the calcium dependency (Shouval et al., 2002). Region is linked to the parameter choice depending on the brain area where the rule is fitted: (C) cortex, (H) hippocampus. The weight-dependency is either modeled by soft bounds (Soft) or hard bounds (Hard). (Ca^{2+}-coupling) The presynaptic calcium influx is coupled with the synaptic weight (Yes/No). The models include an equation considering the depression of presynaptic vesicles labeled short-term depression (STD) (Yes/No). The parameters come from an original paper or are adapted to reproduce the frequency dependency in a pairing protocol (for cortex as in (Sjöström et al., 2001)) or a STDP protocol (for hippocampus as in (Bi and Poo, 1998)).

The homeostatic reset is robust to variability and heterogeneity in circuit parameters

We next tested the robustness of the homeostatic reset to changes in the parameters of the neuronal circuits. We introduced variability in three parameters: (i) the level of neuromodulator concentration, which is modeled by a variable inhibitory drive onto the circuit inhibitory neuron (Figure 3A), (ii) variability in neuron intrinsic parameters such as maximal conductance values (Figure 3B), and (iii) network size, with the introduction of heterogeneity in neuron parameters within the network (Figure 3C).

The results of variability in neuromodulator concentration are shown in Figure 3A. At the circuit level, different concentrations of neuromodulator leads to diverse bursting patterns. These bursting patterns vary in terms of the number of spikes per burst, the intraburst frequency, the interburst frequency and the duty cycle (Jacquerie and Drion, 2021; Drion et al., 2018), which can potentially affect the behavior of the plasticity rules. However, a homeostatic reset of synaptic weights is observed each time the circuit enters a rhythmic mode, and this reset is robust to the specific properties of the pattern itself. A change in the rhythmic pattern solely affects the convergence rate and reset value in the case of soft bounds, and the slope of the linear convergence rate in the case of hard bounds (see Figure 3A, bottom panels, where the different shades of gray represent one circuit simulated with one neuromodulator level). The results show that the homeostatic reset is a robust phenomenon relying on network rhythmic state, but whose reset value is tunable through neuromodulation level.

We then added some variability in order to grow closer to what is observed in biological systems (Jacquerie and Drion, 2021; Marder and Taylor, 2011; Gjorgjieva et al., 2016; Schulz et al., 2006; Marder et al., 1996). To this end, ten circuits varying in their parameter sets of maximal intrinsic conductances and applied currents were simulated. The maximal conductances varied within an interval of 10 %. Each circuit is first verified to switch from tonic to bursting mode. Similarly to neuromodulation level, introducing variability affects the bursting pattern, but also breaks the pattern symmetry between the presynaptic and postsynaptic neurons: each neuron exhibits differences in its neuronal rhythm (Figure 3B, top). This breaking of symmetry does not affect the outcome. In all 10 circuits, whatever the initial weight acquired in tonic mode, the synaptic weights reset in bursting

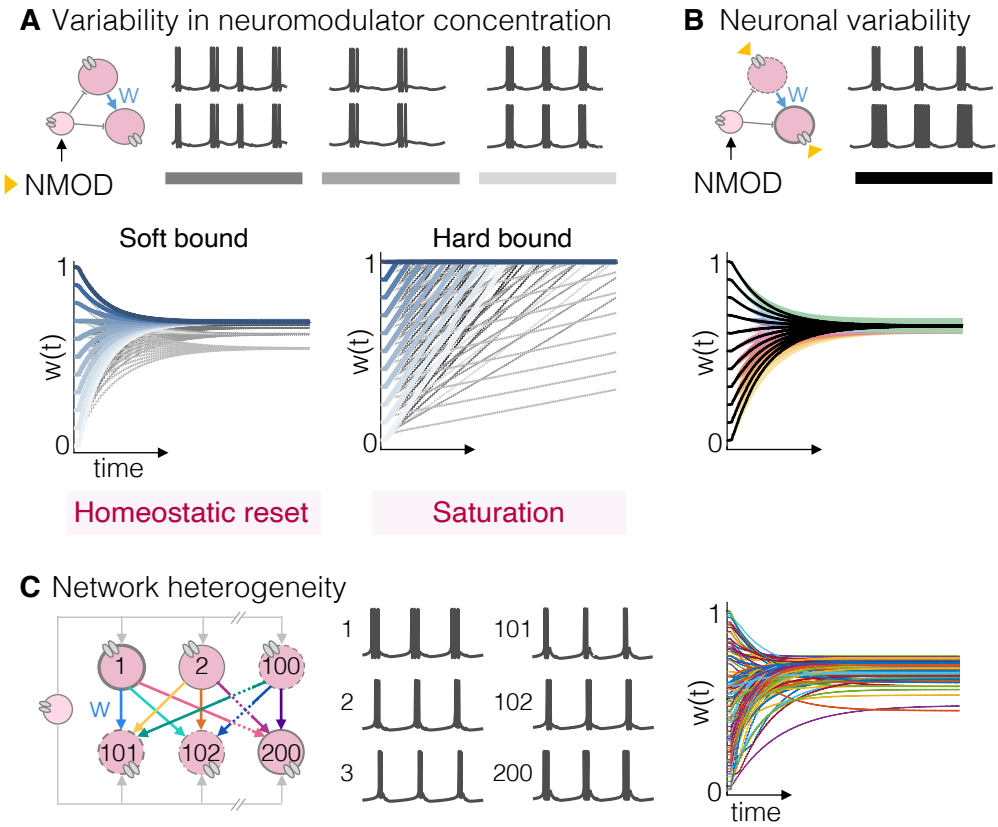

Figure 3: The homeostatic reset occurs for the different category of synaptic plasticity rules and is robust to intrinsic variability and network heterogeneity.
A. Pre- and postsynaptic neurons burst under neuromodulatory input. Different neuromodulator concentrations lead to different bursting patterns (gray line - top traces). The time evolution of the synaptic weight is computed in all synaptic plasticity models considering two weight-dependencies. (Left) Soft bounds lead to a *homeostatic reset* (each blue line is associated to one initial value). The value of the reset is altered by bursting patterns (see gray lines). (Right) For hard bounds, all synaptic weights saturate to the extreme values at different rates depending on the burst profile. (Time window: 40 s.)
B. 10 circuits are generated with variability in their intrinsic parameters affecting the bursting rhythm. Each circuit shows the homeostatic reset. (Averaged weight in black line and its standard deviation in color shadow, time duration: 40 s.).
C. A fully connected feedforward network of 100 pre to 100 postsynaptic neurons is built with heterogeneous intrinsic variability. All initial weights are initialized at random values between 0 and 1. Despite heterogeneity in the network, all synaptic weights present the homeostatic reset and converge towards the same range of values. Each voltage trace lasts 0.9 s - y-scale: 140 mV, 100 weight traces among the 10 000 are shown for model Ca 1, during 50 s.

mode. The exact value of the reset is slightly different in different circuits, as shown in Figure 3B, bottom (the mean evolution of the weights in the 10 circuits is shown in black, whereas the colored shadows depict the standard deviation for each initial condition). The mean reset value is equal to 0.6347 and the standard deviation is equal to 0.0108 for the biophysical model 2. For phenomenological models, the standard deviation is higher due to the sensitivity of the exact spike time inside the intraburst (for the pair-based model: mean = 0.6002, std = 0.0714).

Finally, we increased the network size to account for the impact of heterogeneity between neurons of the same network. We built a heterogeneous network composed of 2 layers of 100 excitatory neurons each fully connected in a feedforward configuration. Each neuron has different intrinsic properties. The inhibitory neuron drives the transition from tonic to burst thanks to the neuromodulatory input (see Figure 3C, left).The network is initialized with random connectivity, mimicking a situation after a learning period (a similar procedure is done in (González-Rueda et al., 2018; Fauth and Van Rossum, 2019). The neurons show different burst rhythms with various intraburst frequencies and different

number of spikes per burst (see Figure 3, center). The evolution of the synaptic weights are displayed in Figure 3C, right. Network heterogeneity induces heterogeneity in reset values within the network. This heterogeneity is related to the variability in pre- and postsynaptic burst properties, it is not dependent on the initial synaptic weight.

Altogether, these different computational experiments convincingly show that the mechanisms underlying the homeostatic reset of synaptic weights are robust to synaptic model type, the fitted region, the presence of short-term depression, the neuromodulation level, the neuronal circuit variability and the network heterogeneity. In all cases, strong weights decrease and weak weights grow toward a reset value. This exact value is moderately influenced by rhythm properties, hence tunable by neuromodulator level. Turning soft-bound into hard bound simply drives all the weights toward saturation.

The endogenous nature of rhythmic bursting leads to homeostatic reset

In order to gain more insights into the mechanisms underlying the homeostatic reset, and particularly understand why this phenomenon specifically occurs during bursting activity observed in quiet waking state, we analyzed how phenomenological and biophysical plasticity models interact with circuit activity. In particular, we took advantage of previous analytical work linking the time evolution and convergence of synaptic weights to either spike time statistics (for phenomenological models) or calcium dynamics (for biophysical models) (Billings and van Rossum, 2009; Jędrzejewska-Szmek et al., 2017; Babadi and Abbott, 2016; Rubin et al., 2001; Park et al., 2017).

In phenomenological models, the time evolution of a synaptic weight and its convergence occurs on a time interval much larger than typical interspike intervals. Therefore, following the work of (Gütig et al., 2003; Legenstein and Maass, 2005), we can average the dynamics of the synaptic weight (see (1) in Materials and Methods) over a time interval T and get

$$\dot{w} = -A^- w^\mu \int_{-\infty}^{0} e^{s/\tau^-} C(s;t)ds + A^+(1-w)^\mu \int_{0}^{\infty} e^{-s/\tau^+} C(s;t)ds,$$

where A^+ and A^- are the potentiation and depression parameters, μ stands for the weight-dependency, $e^{-|s|/\tau^\pm}$ stands for the STDP kernel in potentiation or depression with τ^+ and τ^- being the time-constants given in the pair-based model, and $C(s;t)$ is the (temporally averaged) correlation function between the pre and post spike trains, respectively noted $S_{\text{pre}}(t) = \sum_k \delta(t - t_{\text{pre},k})$ and $S_{\text{post}}(t) = \sum_k \delta(t - t_{\text{post},k})$, that is,

$$C(s;t) = \frac{1}{T}\int_{t}^{t+T} S_{\text{pre}}(\tau) S_{\text{post}}(\tau + s)d\tau.$$

Assuming the stationarity of both spike trains, the correlation function is time-invariant, *i.e.*, $C(s;t) = C(s)$, and the time evolution of the synaptic weight can be computed as (Legenstein and Maass, 2005):

$$\dot{w} = A^+(1-w)^\mu C^+ - A^- w^\mu C^-,$$

where $C^+ = \int_0^\infty e^{-s/\tau^+} C(s)ds$ and $C^- = \int_{-\infty}^0 e^{s/\tau^-} C(s)ds$.

A qualitative analysis of this equation helps to understand why synaptic weights converge towards a single steady-state for any stationary value of $C(s)$, considering soft-bound dependency *i.e.* $\mu = 1$. The term $A^+(1-w)C^+$ computes the weight increase due to all postsynaptic spikes following presynaptic spikes considering the associated time lag. The term $A^- wC^-$ computes the weight decrease due to all postsynaptic spikes preceding presynaptic spikes. When modeling soft bounds, both terms are weight-dependent, which deforms the plasticity kernel (Figure 4A). When the synaptic weight is weak, the term $A^+(1-w)C^+$ dominates, and potentiation overcomes depression (Figure 4A, left). When the synaptic weight is strong, the term $A^- wC^-$ dominates, and depression overcomes potentiation (Figure 4A, center). The drift eventually stabilizes at the synaptic weight value for which depression balances potentiation, *i.e.*, $A^+(1-w)C^+ = A^- wC^-$ (Figure 4A, right). This convergence value can be computed analytically by solving this balance equation.The reset value w_{HR} is obtained analytically

by

$$w_{\mathrm{HR}} = \frac{\frac{A^+C^+}{A^-C^-}}{1 + \frac{A^+C^+}{A^-C^-}}. \tag{3}$$

This equation states that the reset value depends on a ratio between the potentiation parameter weighted by the correlation between pre-post spikes and the depression parameter weighted by the correlation between post-pre spikes.

We applied this methodology to compare the convergence of the synaptic weights in tonic spiking and bursting. To this end, we used the previously built heterogeneous network composed of 2 layers of 100 excitatory neurons fully connected in a feedforward configuration (Figure 4B). The network is initialized with random connectivities. In tonic mode, excitatory neurons receive external stimulation at random frequencies, ranging from 0.01 Hz up to 50 Hz, which mimics the effect of sensory drive, among others (Figure 4B, top). In bursting mode, a neuromodulatory drive to the inhibitory cell switches the network to rhythmic mode (Figure 4B, bottom).

First, we computed the correlation ratio C^+/C^- between the pre and post (binary) spike trains for all 10 000 synaptically coupled pairs, both in tonic and burst modes. The results are reported in a correlation matrix for each mode (Figure 4C, left). These correlation matrices show that correlation values are highly heterogeneous in tonic mode, whereas they are highly homogeneous in burst mode. This is due to the fact that spike trains are variable during active waking, whereas the network switches to a global, rhythmic activity during quiet waking mode (Figure 4C, center). As a consequence, synaptic weights are predicted to converge towards many different values during tonic mode, but towards very similar values in bursting mode, which partially explains why the homeostatic reset is only observed during the latter.

Secondly, we compared the synaptic weight values obtained from model simulations with the prediction values w_{HR}. Prediction values were computed on the complete time period T, as well as on two transient time periods T_1 and T_2, and results are provided on a raster plot for each time period in both modes (Figure 4C, right, mean prediction error $\pm$ standard deviation over 8 different neuromodulator drives: mean = 0.0031, std = 0.0027, see *SI Appendix* for details). The figures show that, although there is an almost perfect match between simulated and predicted reset values in bursting mode, simulated synaptic weights do not converge towards their predicted values during tonic mode for any time window. This is explained by the assumption that the correlation function between the spike trains is stationary over the time windows, *i.e.*, $C(s;t) \approx C(s)$, is only true in bursting mode, due to the endogenous nature of the rhythmic bursting activity. As a result, a reset of synaptic weights is only really observed during quiet waking.

In biophysical models, a similar analytical approach can be derived based on calcium dynamics by comparing the time spent in depression and potentiation (Graupner and Brunel, 2012). Again the time evolution of a synaptic weight and its convergence occur on a time interval much larger than typical calcium oscillations. Therefore, we can average the dynamics of the synaptic weight (see (2) in Materials and Methods) over a time interval T and get

$$\dot{w} = \frac{1}{T}\int_t^{t+T} \frac{1}{\tau_w([\mathrm{Ca}](s))}\left[\Omega([\mathrm{Ca}](s)) - \mu\, w\right] ds,$$

where $\Omega([\mathrm{Ca}])$ and $\tau_w([\mathrm{Ca}])$ are functions that map intracellular calcium concentration to potentiation (Ω^{p}) and depression (Ω^{d}) levels and potentiation (τ_{p}) and depression (τ_{d}) time-constants, as in (Graupner et al., 2016) (see *SI Appendix*). We note the effective time spent in each region α^{d} and α^{p} as the time spent balanced by the time-constant of potentiation/depression in the corresponding region, that is,

$$\alpha^{\mathrm{d}} = \frac{1}{\tau_{\mathrm{d}}}\frac{1}{T}\int_t^{t+T} I(\theta_{\mathrm{d}} < [\mathrm{Ca}](s) < \theta_{\mathrm{p}})ds,$$
$$\alpha^{\mathrm{p}} = \frac{1}{\tau_{\mathrm{p}}}\frac{1}{T}\int_t^{t+T} I([\mathrm{Ca}](s) > \theta_{\mathrm{p}})ds,$$

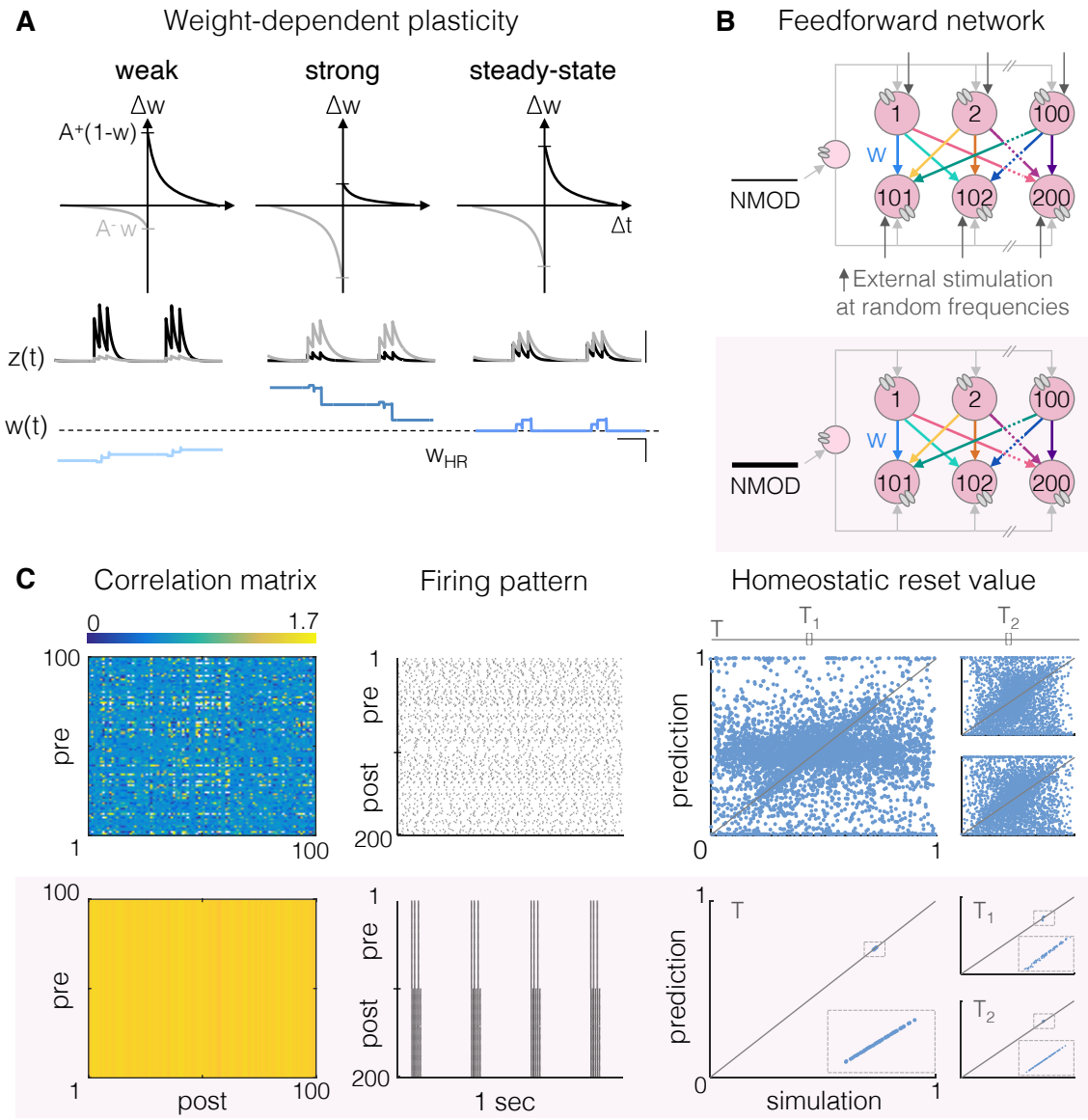

Figure 4: The homeostatic reset relies on the endogenous nature of rhythmic bursting.
A. Weight-dependent plasticity modulates the potentiation and depression parameters with respect to the synaptic weights. The spike-time dependent plasticity kernel is weight-dependent. The potentiation and depression traces (z(t)) are shown respectively in black and gray with the associated synaptic weight evolution (w(t)) considering two successions of endogenous burst (x-scale: 0.6 s, y-scale for z: 0.06 %, y-scale for w: 2.5 %.)
B. A 2-layer feedforward network with the same 100 neurons fully connected to the same 100 postsynaptic neurons. All the synaptic weights (resp. AMPA connections) are randomly initialized between 0 to 1 (resp. 0.01 to 4). In tonic spiking (top, white background), neurons are excited by external stimulation at random frequencies between 0.01 to 50 Hz. In bursting mode (bottom, pink background), the neuromodulation (NMOD) level drives the neurons in burst mode.
C. (Left) The correlation between presynaptic spike trains and postsynaptic spike trains are computed. We show the ratio between the positive correlation (C^+ associates to the potentiation correlation when a postsynaptic neuron spikes after a presynaptic neuron) and the negative correlation (C^- for a pre spikes after a post spikes) in tonic spiking and bursting (resp. top white background and bottom pink background). (Center, top) In tonic mode, neurons are in exogenous spiking mode. (Center, bottom) In bursting mode, neurons are in endogenous burst mode. (Right) The spike trains correlation is computed for the entire simulation T and compared with the correlation at two given times T_1 and T_2 (equal to 10 s and 40 s). Scatter plots between the reset value obtained via simulation (converging point) and the predicted value obtained analytically.

where $I(x)$ is the indicator function equals 1 when x is true and 0 when x is false. The synaptic weights reach a stable state once the potentiation level Ω^{p} and the depression level Ω^{d} weighted by

their effective time spent in the corresponding regions are balanced. It gives

$$w_{\mathrm{HR}} = \frac{\Omega^{\mathrm{d}}\alpha^{\mathrm{d}} + \Omega^{\mathrm{p}}\alpha^{\mathrm{p}}}{\alpha^{\mathrm{d}} + \alpha^{\mathrm{p}}}. \tag{4}$$

The comparison between the value of the homeostatic reset obtained via computational simulations and the analytic approach is provided in *SI Appendix, Tab.S7*. Again, w_{HR} is only predictive if the effective time spent in each region α^{d} and α^{p} can be considered stable over time, which is only true in bursting mode, as attested by the good match between predicted and simulated reset values (mean prediction error $\pm$ standard deviation over 8 different neuromodulatory drives: mean error = 0.0016, std = 0.0019)).

Finally, both analytical analyses can be extended to the case of hard bounds. In this case, all synaptic weights converge towards saturation in quiet waking mode due to burst mode, and the saturation speed λ, or slope, depends on the neuromodulatory drive. In phenomenological models, this saturation slope can be predicted by the equation

$$\lambda = A^{+}C^{+} - A^{-}C^{-},$$

where T is the time-window considered to compute the correlation. In biophysical models, the saturation slope corresponds to the sum of the depression rate and potentiation rate, each weighted by the fraction of time spent in their corresponding regions α^{d} and α^{p}, which writes

$$\lambda = \alpha^{\mathrm{p}}\Omega^{\mathrm{p}} + \alpha^{\mathrm{d}}\Omega^{\mathrm{d}}.$$

The values of the saturation slope obtained via computational simulations match the analytic predictions for both model types (*SI Appendix, Tab. S7* - calcium model: mean error = 0.049, std = 0.039, pair-based model: mean error = 0.027, std = 0.033 over 8 neuromodulatory drives). Complementary explanations about the origin of the homeostatic reset are available in *SI Appendix.*

In summary, analytical analyses of the mechanisms underlying time evolution of synaptic weights showed that a homeostatic reset solely occurs during quiet waking mode due to the endogenous, global nature of the network rhythmic bursting activity in this mode, both in phenomenological models and biophysical models of synaptic plasticity.

The homeostatic reset is robust to neuromodulation of synaptic plasticity rules

Recent evidence shows that synaptic plasticity rules are also under the control of neuromodulators for example, acetylcholine, dopamine, noradrenaline, serotonin, and histamine (Brzosko et al., 2019; Zannone et al., 2018; Foncelle et al., 2018; Salgado et al., 2012; Nadim and Bucher, 2014; Lisman et al., 2011; Pawlak, 2010; Kirkwood, 2007; Shine et al., 2021; Gerstner et al., 2018; Izhikevich, 2007). Neuromodulators are affecting synaptic plasticity at different stages as explained in (Seol et al., 2007; Bazzari and Parri, 2019; Nadim and Bucher, 2014; Pawlak, 2010). Several computational models were developed in the last years in different fields of neuroscience implementing this notion of neuromodulated synaptic plasticity rules (Butson, 2012; Frémaux and Gerstner, 2015). For example, in the context of sleep-dependent memory consolidation (González-Rueda et al., 2018), the classical depression-potentiation kernel in wakefulness is deformed into a depression kernel in sleep to show weight downselection. A similar modeling approach is done in (Brzosko et al., 2017; Pedrosa and Clopath, 2017). The STDP kernel is sequentially shifted due to dopamine and acetylcholine for reward-based navigation or to explore receptive field plasticity. There exist other computational techniques to incorporate neuromodulation in synaptic plasticity rules such as the introduction of an eligibility trace or a third factor (Gerstner et al., 2018; Izhikevich, 2007; Foncelle et al., 2018).

Inspired by this line of work, we introduced neuromodulation of synaptic plasticity rules to test its effect during rhythmic bursting activity and on the homeostatic reset. In phenomenological plasticity rules, it is simply translated by modifications of the rule parameters (Figure 5A, top-left). Based on (3), modifying the potentiation or depression parameters (A^{+} and A^{-}) has a direct effect on the homeostatic reset value. To confirm our analytical predictions, we simulated the circuit during bursting

activity with different initial synaptic weights (as done in Figure 3A) and compared the reset value with and without neuromodulation on the synaptic plasticity rule (as shown respectively by yellow and blue curves, Figure 5B, top-right). The homeostatic reset is robust and neuromodulation only affects its set point. For calcium-based plasticity rules, neuromodulators can similarly target several parameters such the potential and depression levels (Ω^{p} and Ω^{d}) (see in Figure 5A, bottom-left). As given in the analytical expression of the homeostatic reset value in (4), modifying those parameters changes the value whatever the initial weight. Figure 5A (bottom-right) confirms the prediction through the computational experiment. For both rule categories, other parameters can be modulated and the results are provided in *SI appendix*. Overall, neuromodulating the synaptic plasticity rule does not disrupt the homeostatic reset.

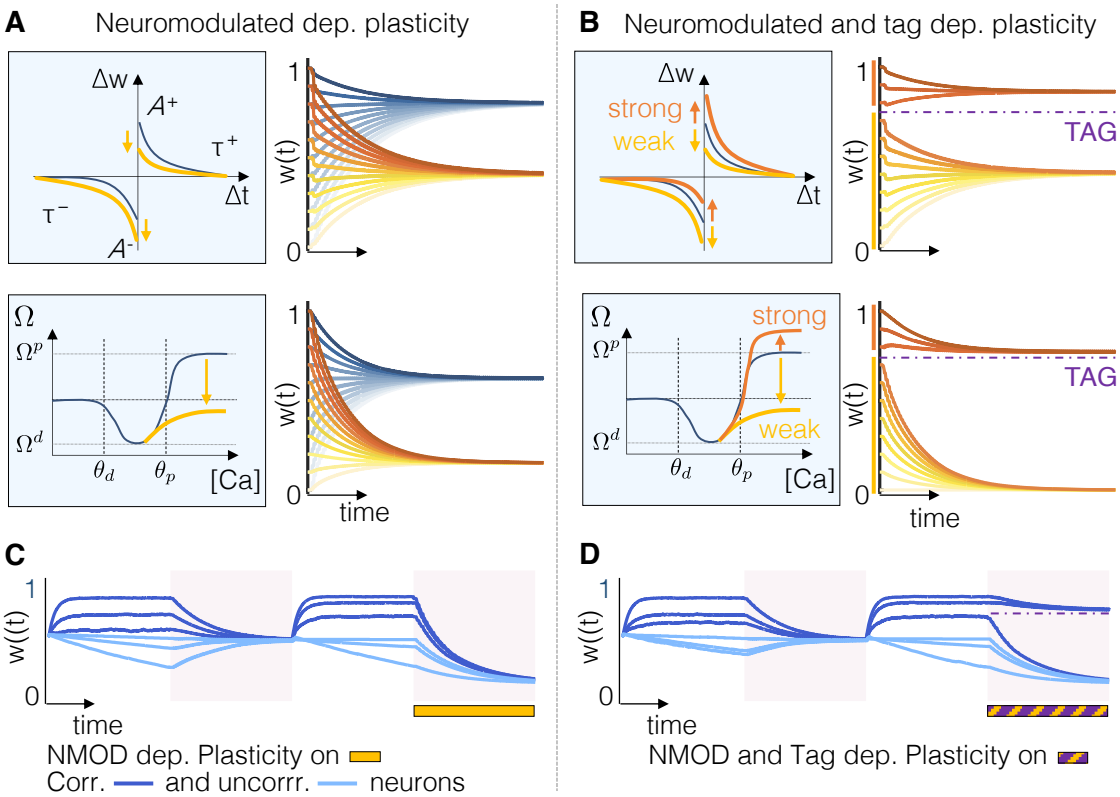

Figure 5: Neuromodulated and tag-dependent synaptic plasticity rules exploit the burst-induced homeostatic reset for memory consolidation.
A. Phenomenological (top, right) and calcium-based (bottom, right) plasticity rules are neuromodulated by changing the potentiation and depression paramters (respectively A^+, A^- and Ω^{p}). Time-evolution of the synaptic weights when the synaptic rule is neuromodulated (yellow curves) or not (blue curves - similar as shown in Figure 3). The homeostatic reset is moved. **B.** (left) Parameters are neuromodulated according to the weight acquired during learning (here the initial weights). Strong weights ($w>$ TAG, indicated by the purple line) follow the plasticity rule drawn in orange while weak weights follow the rule drawn in yellow. (right) Time-evolution of the synaptic weights when the synaptic rule is neuromodulated and tag-dependent. Strong weights are preserved while weak weights are depressed as shown by two resets at high and low values in a phenomenological (top) and calcium-based (bottom) rule. (x-scale: 10 s, simulation duration: 40 s). **C and D.** Evolution of the synaptic weights in 6 circuits during two tonic-burst transitions (as done in Figure 1B, white background for tonic firing and pink background for bursting) except that the last stage is either under a neuromodulated plasticity rule (C, indicated by the yellow bar) or neuromodulated and tag-dependent plasticity rule (D, indicated by the yellow and purple bars). Half of the circuits have correlated activity (dark blue lines) and the rest have uncorrelated activity (light blue lines). The homeostatic reset is robust to neuromodulation but can be exploited to provide a bimodal convergence thanks to a tagging mechanism (30 s by state, total simulation 120 s).

However, now that we have presented a mechanism to tune the value of the reset, it can be leveraged to obtain a bimodal behavior in the evolution of the synaptic weights during the rhythmic

bursting regime, hence permitting memory consolidation. In such bimodal behavior, strong weights would converge to a high reset value while weak values are downscaled to a low reset value. This idea is perfectly in line with the synaptic-and-capture hypothesis (STC) (Seibt and Frank, 2019; Okuda et al., 2021). To implement this hypothesis in the different synaptic rules, the parameters are required to be dependent on the weight acquired during the learning phase. The strong weights formed during the correlated learning activity create the potential for consolidation by setting a *TAG*. A connection is tagged when the weight acquired during learning is higher than a threshold value (Frey and Morris, 1997; Redondo and Morris, 2011; Seibt and Frank, 2019). For tagged connections, the potentiation parameter has a higher value compared to weak weights leading to a higher reset point. It was shown in phenomenological and calcium-based rules in Figure 5B (respectively top and bottom). As soon as the neurons switch in rhythmic bursting mode, synaptic weights are converging towards their reset values but this time dictated by the presence of the TAG (see Figure 5B, right).

Figures 5C and D repeat the experiment done in Figure 1B expect that during the last bursting state, the synaptic plasticity rule is neuromodulated (Figure 5C) or neuromodulated and tag-dependent (Figure 5D). It confirms that the burst-induced homeostatic reset is robust to alteration in the synaptic plasticity rules. At the last bursting stage, the weights converge to a low reset point altogether in Figure 5C. The only way to exploit it is to build a TAG-dependent rule as done in Figure 5D where weights that are strong enough are maintained. It suggests a potential function for the role of burst and its associated homeostatic reset for consolidation of strong weights acquired during learning.

Discussion

A key step in understanding how switches in brain states affect memory encoding is finding ways to study the interactions between synaptic plasticity rules and neuromodulation of brain activity. It represents a challenge, as plasticity rules and neuromodulation target neurons at the molecular and cellular levels, whereas brain states and memory emerge at the population level. In this work, we leverage the power of computational modeling to study how network connections formed via any of 20 variations of 7 well-established plasticity rules are affected by a switch from asynchronous tonic spiking to rhythmic bursting, mimicking transitions between active and quiet waking states. We showed that transitions to quiet waking induce a homeostatic reset of all synaptic weights towards a specific value for all tested synaptic plasticity rules.

For a newly described phenomenon in a computational modeling work to be of physiological relevance, it has to be shown that it does not arise from an artifact of the choice of models and parameters used in the study. We therefore thoroughly tested the robustness of the homeostatic reset to variability in models and parameters. First, we showed that the homeostatic reset arises from both phenomenological models and biophysical models of synaptic plasticity, which ruled out the possibility of an artifact of the chosen model type. Second, the homeostatic reset was shown to be robust to changes in neuromodulator drive, variability in neuron and circuit parameters, and heterogeneity in larger neuronal populations. Changes in neuromodulator drive however affected the reset value, which suggests that the homeostatic reset is both a robust and tunable phenomenon. Finally, using mathematical analyses that directly link firing activity or calcium dynamics to changes in synaptic weights, we showed that the homeostatic reset is limited to the quiet waking period due to the highly endogenous, rhythmic activity globally shared by the network during that period.

The main effect of the homeostatic reset is that it restores synaptic weights during quiet waking regardless of their evolution during learning. The consequences of this restoration are twofold. On the one hand, it provides a mechanism by which synaptic weight returns to a homeostatic set point between two learning periods, restoring the ability of the network to learn new information. Such a mechanism could play a central role in memory homeostasis. On the other hand, the homeostatic reset disrupts any learning that occurred during the previous period, which could lead to catastrophic forgetting (González et al., 2020). This forgetting may be overcome via mechanisms that transfer learning encoded in synaptic weight into long-lasting, structural changes in synaptic connections, such as the number of receptors at each synapse, the number and size of synapses, etc (Zenke and Gerstner, 2017;

Luboeinski and Tetzlaff, 2021). Another possibility would be to exploit the homeostatic reset itself through neuromodulator-induced changes in synaptic rules (Pedrosa and Clopath, 2017; González-Rueda et al., 2018; Foncelle et al., 2018; Brzosko et al., 2017). We have however shown that such a mechanism would need to take into account the history of weight evolution to permit a bimodal behavior of synaptic weights, which is a quite strong requirement. This could however be potentially achieved following the synaptic tagging hypothesis.

References

Abbott LF, Nelson SB (2000) Synaptic plasticity: Taming the beast. *Nature Neuroscience* 3:1178–1183.

Babadi B, Abbott LF (2016) Stability and Competition in Multi-spike Models of Spike-Timing Dependent Plasticity. *PLoS Computational Biology* 12.

Bazhenov M, Timofeev I, Steriade M, Sejnowski TJ (2002) Model of thalamocortical slow-wave sleep oscillations and transitions to activated states. *Journal of Neuroscience* 22:8691–8704.

Bazzari A, Parri H (2019) Neuromodulators and Long-Term Synaptic Plasticity in Learning and Memory: A Steered-Glutamatergic Perspective. *Brain Sciences* 9:300.

Bezanson J, Edelman A, Karpinski S, Shah VB (2017) Julia: A Fresh Approach to Numerical Computing. *SIAM Review* 59:65–98.

Bi GQ, Poo MM (1998) Synaptic modifications in cultured hippocampal neurons: Dependence on spike timing, synaptic strength, and postsynaptic cell type. *Journal of Neuroscience* 18:10464–10472.

Billings G, van Rossum MCW (2009) Memory Retention and Spike-Timing-Dependent Plasticity. *Journal of Neurophysiology* 101:2775–2788.

Brzosko Z, Mierau SB, Paulsen O (2019) Neuromodulation of Spike-Timing-Dependent Plasticity: Past, Present, and Future. *Neuron* 103:563–581 Publisher: Elsevier Inc.

Brzosko Z, Zannone S, Schultz W, Clopath C, Paulsen O (2017) Sequential neuromodulation of Hebbian plasticity offers mechanism for effective reward-based navigation. *eLife* 6:e27756.

Butson CR (2012) Computational Models of Neuromodulation. *International Review of Neurobiology* 107:5–22.

Buzsáki G (1998) Memory consolidation during sleep: a neurophysiological perspective. *Journal of Sleep Research* 7:17–23.

Cannon J, Mccarthy MM, Lee S, Lee J, Börgers C, Whittington MA, Kopell N (2014) Neurosystems: Brain rhythms and cognitive processing. *European Journal of Neuroscience* 39:705–719.

Chen JY, Lonjers P, Lee C, Chistiakova M, Volgushev M, Bazhenov M (2013) Heterosynaptic plasticity prevents runaway synaptic dynamics. *Journal of Neuroscience* 33:15915–15929.

Chrol-Cannon J, Jin Y (2014) Computational modeling of neural plasticity for self-organization of neural networks. *Biosystems* 125:43–54.

Citri A, Malenka RC (2008) Synaptic plasticity: Multiple forms, functions, and mechanisms. *Neuropsychopharmacology* 33:18–41.

Dastgheib M, Kulanayagam A, Dringenberg HC (2022) Is the role of sleep in memory consolidation overrated? *Neuroscience & Biobehavioral Reviews* 140:104799.

Deperrois N, Graupner M (2020) Short-term depression and long-term plasticity together tune sensitive range of synaptic plasticity. *PLoS Computational Biology* 16:1–25.

Drion G, Dethier J, Franci A, Sepulchre R (2018) Switchable slow cellular conductances determine robustness and tunability of network states. *PLoS Computational Biology* 14:1–20.

Fauth MJ, Van Rossum MC (2019) Self-organized reactivation maintains and reinforces memories despite synaptic turnover. *eLife* 8:1–19.

Foncelle A, Mendes A, Jędrzejewska-Szmek J, Valtcheva S, Berry H, Blackwell KT, Venance L (2018) Modulation of spike-timing dependent plasticity: Towards the inclusion of a third factor in computational models. *Frontiers in Computational Neuroscience* 12:1–21.

Frey U, Morris RGM (1997) Synaptic tagging and long-term potentiation. *Nature* 385:533–536.

Frémaux N, Gerstner W (2015) Neuromodulated spike-timing-dependent plasticity, and theory of three-factor learning rules. *Frontiers in Neural Circuits* 9.

Gerstner W (2011) Hebbian Learning and Plasticity. *From neuron to cognition via computational neuroscience* pp. 1–25.

Gerstner W, Kistler WM (2002) Mathematical formulations of Hebbian learning. *Biological Cybernetics* 87:404–415.

Gerstner W, Lehmann M, Liakoni V, Corneil D, Brea J (2018) Eligibility Traces and Plasticity on Behavioral Time Scales: Experimental Support of NeoHebbian Three-Factor Learning Rules. *Frontiers in Neural Circuits* 12:1–16.

Gjorgjieva J, Drion G, Marder E (2016) Computational implications of biophysical diversity and multiple timescales in neurons and synapses for circuit performance. *Current Opinion in Neurobiology* 37:44–52 Publisher: Elsevier Ltd.

González OC, Sokolov Y, Krishnan GP, Delanois JE, Bazhenov M (2020) Can sleep protect memories from catastrophic forgetting? *eLife* 9.

González-Rueda A, Pedrosa V, Feord RC, Clopath C, Paulsen O (2018) Activity-Dependent Downscaling of Subthreshold Synaptic Inputs during Slow-Wave-Sleep-like Activity In Vivo. *Neuron* 97:1244–1252.e5.

Graupner M, Brunel N (2012) Calcium-based plasticity model explains sensitivity of synaptic changes to spike pattern, rate, and dendritic location. *Proceedings of the National Academy of Sciences of the United States of America* 109:3991–3996.

Graupner M, Wallisch P, Ostojic S (2016) Natural firing patterns imply low sensitivity of synaptic plasticity to spike timing compared with firing rate. *Journal of Neuroscience* 36:11238–11258.

Gütig R, Aharonov R, Rotter S, Sompolinsky H (2003) Learning Input Correlations through Nonlinear Temporally Asymmetric Hebbian Plasticity. *The Journal of Neuroscience* 23:3697–3714.

Heidelberger R, Shouval H, Zucker RS, Byrne JH (2014) Synaptic Plasticity In *From Molecules to Networks: An Introduction to Cellular and Molecular Neuroscience: Third Edition*, pp. 533–561. Elsevier Inc.

Hill S, Tononi G (2005) Modeling sleep and wakefulness in the thalamocortical system. *Journal of Neurophysiology* 93:1671–1698.

Humphries M (2012) Dopaminergic control of the exploration-exploitation trade-off via the basal ganglia. *Frontiers in Neuroscience* 6.

Izhikevich EM (2007) Solving the distal reward problem through linkage of STDP and dopamine signaling. *Cerebral Cortex* 17:2443–2452.

Jacquerie K, Drion G (2021) Robust switches in thalamic network activity require a timescale separation between sodium and T-type calcium channel activations. *PLOS Computational Biology* 17:e1008997.

Jędrzejewska-Szmek J, Damodaran S, Dorman DB, Blackwell KT (2017) Calcium dynamics predict direction of synaptic plasticity in striatal spiny projection neurons. *European Journal of Neuroscience* 45:1044–1056.

Kirkwood A (2007) Neuromodulation of Cortical Synaptic Plasticity In Tseng KY, Atzori M, editors, *Monoaminergic Modulation of Cortical Excitability*, pp. 209–216. Springer US, Boston, MA.

Kühn AA, Williams D, Kupsch A, Limousin P, Hariz M, Schneider GH, Yarrow K, Brown P (2004) Event-related beta desynchronization in human subthalamic nucleus correlates with motor performance. *Brain* 127:735–746.

Legenstein RA, Maass W (2005) A Criterion for the Convergence of Learning with Spike Timing Dependent Plasticity In *NIPS 2005*, p. 8, Vancouver, Canada.

Lisman J, Grace AA, Duzel E (2011) A neoHebbian framework for episodic memory; role of dopamine-dependent late LTP. *Trends in Neurosciences* 34:536–547.

Luboeinski J, Tetzlaff C (2021) Memory consolidation and improvement by synaptic tagging and capture in recurrent neural networks. *Communications Biology* 4:275.

Marder E, Abbott LF, Turrigiano GG, Liu Z, Golowasch J (1996) Memory from the dynamics of intrinsic membrane currents. *Proceedings of the National Academy of Sciences of the United States of America* 93:13481–13486.

Marder E, Taylor AL (2011) Multiple models to capture the variability in biological neurons and networks. *Nature Neuroscience* 14:133–138 Publisher: Nature Publishing Group.

Mazzoni A, Lindén H, Cuntz H, Lansner A, Panzeri S, Einevoll GT (2015) Computing the Local Field Potential (LFP) from Integrate-and-Fire Network Models. *PLOS Computational Biology* 11:e1004584.

McCormick DA, Bal T (1997) Sleep and arousal: Thalamocortical mechanisms. *Annual Review of Neuroscience* 20:185–215.

McCormick DA, Salkoff DB (2015) Brain State Dependent Activity in the Cortex and Thalamus. *Current Opinion in Neurobiology* 31:133–140.

McGinley MJ, Vinck M, Reimer J, Batista-Brito R, Zagha E, Cadwell CR, Tolias AS, Cardin JA, McCormick DA (2015) Waking State: Rapid Variations Modulate Neural and Behavioral Responses. *Neuron* 87:1143–1161 Publisher: Elsevier.

Morrison A, Diesmann M, Gerstner W (2008) Phenomenological models of synaptic plasticity based on spike timing. *Biological Cybernetics* 98:459–478.

Nadim F, Bucher D (2014) Neuromodulation of neurons and synapses. *Current Opinion in Neurobiology* 29:48–56.

Okuda K, Højgaard K, Privitera L, Bayraktar G, Takeuchi T (2021) Initial memory consolidation and the synaptic tagging and capture hypothesis. *European Journal of Neuroscience* 54:6826–6849.

Olcese U, Esser SK, Tononi G (2010) Sleep and synaptic renormalization: A computational study. *Journal of Neurophysiology* 104:3476–3493.

Park Y, Choi W, Paik SB (2017) Symmetry of learning rate in synaptic plasticity modulates formation of flexible and stable memories. *Scientific Reports* 7:5671.

Pawlak V (2010) Timing is not everything: neuromodulation opens the STDP gate. *Frontiers in Synaptic Neuroscience* 2.

Pedrosa V, Clopath C (2017) The role of neuromodulators in cortical plasticity. A computational perspective. *Frontiers in Synaptic Neuroscience* 8:38–38.

Pfister JP, Gerstner W (2006) Triplets of spikes in a model of spike timing-dependent plasticity. *Journal of Neuroscience* 26:9673–9682.

Redondo RL, Morris RGM (2011) Making memories last: the synaptic tagging and capture hypothesis. *Nature Reviews Neuroscience* 12:17–30.

Reimer J, Froudarakis E, Cadwell C, Yatsenko D, Denfield G, Tolias A (2014) Pupil Fluctuations Track Fast Switching of Cortical States during Quiet Wakefulness. *Neuron* 84:355–362.

Rubin J, Lee DD, Sompolinsky H (2001) Equilibrium Properties of Temporally Asymmetric Hebbian Plasticity. *Physical Review Letters* 86:364–367.

Salgado H, Köhr G, Treviño M (2012) Noradrenergic 'Tone' Determines Dichotomous Control of Cortical Spike-Timing-Dependent Plasticity. *Scientific Reports* 2:417.

Schulz DJ, Goaillard JM, Marder E (2006) Variable channel expression in identified single and electrically coupled neurons in different animals. *Nature Neuroscience* 9:356–362.

Seibt J, Frank MG (2019) Primed to sleep: The dynamics of synaptic plasticity across brain states. *Frontiers in Systems Neuroscience* 13:1–19.

Seol GH, Ziburkus J, Huang S, Song L, Kim IT, Takamiya K, Huganir RL, Lee HK, Kirkwood A (2007) Neuromodulators Control the Polarity of Spike-Timing-Dependent Synaptic Plasticity. *Neuron* 55:919–929.

Sherman SM (2001) Tonic and burst firing: dual modes of thalamocortical relay. *Trends in neurosciences* 24:122–6.

Sherman SM, Guillery RW (1996) Functional organization of thalamocortical relays. *Journal of Neurophysiology* 76:1367–1395.

Shine JM, Müller EJ, Munn B, Cabral J, Moran RJ, Breakspear M (2021) Computational models link cellular mechanisms of neuromodulation to large-scale neural dynamics. *Nature Neuroscience* 24:765–776.

Shouval HZ, Bear MF, Cooper LN (2002) A unified model of NMDA receptor-dependent bidirectional synaptic plasticity. *Proceedings of the National Academy of Sciences of the United States of America* 99:10831–10836.

Sjöström PJ, Turrigiano GG, Nelson SB (2001) Rate, Timing, and Cooperativity Jointly Determine Cortical Synaptic Plasticity. *Neuron* 32:1149–1164.

Song S, Miller KD, Abbott LF (2000) Competitive Hebbian learning through spike-timing-dependent synaptic plasticity. *Nature Neuroscience* 3:919–926.

Steriade M, Timofeev I, Grenier F (2001) Natural waking and sleep states: A view from inside neocortical neurons. *Journal of Neurophysiology* 85:1969–1985.

Telenczuk B, Telenczuk M, Destexhe A (2020) A kernel-based method to calculate local field potentials from networks of spiking neurons. *Journal of Neuroscience Methods* 344:108871.

van Rossum MCW, Shippi M, Barrett AB (2012) Soft-bound Synaptic Plasticity Increases Storage Capacity. *PLoS Computational Biology* 8:e1002836.

Van Rossum MC, Bi GQ, Turrigiano GG (2000) Stable Hebbian learning from spike timing-dependent plasticity. *Journal of Neuroscience* 20:8812–8821.

Vyazovskiy VV, Olcese U, Hanlon EC, Nir Y, Cirelli C, Tononi G (2011) Local sleep in awake rats. *Nature* 472:443–447.

Zagha EM D (2014) Neural Control of Brain State. *Current Opinion in NeurobiologyBiology* 0:178–186 ISBN: 6176321972 _eprint: NIHMS150003.

Zagha E, McCormick DA (2014) Neural control of brain state. *Current Opinion in Neurobiology* 29:178–186 Publisher: Elsevier Ltd.

Zannone S, Brzosko Z, Paulsen O, Clopath C (2018) Acetylcholine-modulated plasticity in reward-driven navigation: a computational study. *Scientific Reports* 8:1–20.

Zenke F, Gerstner W (2017) Hebbian plasticity requires compensatory processes on multiple timescales. *Philosophical Transactions of the Royal Society B: Biological Sciences* 372.